

This discussion paper is/has been under review for the journal Geoscientific Model Development (GMD). Please refer to the corresponding final paper in GMD if available.

The mid-Pliocene climate simulated by FGOALS-g2

W. Zheng¹, Z. Zhang^{2,3}, L. Chen^{1,4}, and Y. Yu¹

¹State Key Laboratory of Numerical Modeling for Atmospheric Sciences and Geophysical Fluid Dynamics (LASG), Institute of Atmospheric Physics, Chinese Academy of Sciences, Beijing 100029, China

²Nansen-Zhu International Research Centre (NZC), Institute of Atmospheric Physics, Chinese Academy of Sciences, Beijing 100029, China

³UniResearch, Bjerknes Centre for Climate Research, Bergen 5007, Norway

⁴University of Chinese Academy of Sciences, Beijing 100049, China

Received: 8 March 2013 – Accepted: 25 March 2013 – Published: 9 April 2013

Correspondence to: W. Zheng (zhengwp@mail.iap.ac.cn)

Published by Copernicus Publications on behalf of the European Geosciences Union.

GMDD

6, 2403–2428, 2013

The mid-Pliocene
climate simulated by
FGOALS-g2

W. Zheng et al.

Title Page

Abstract

Introduction

Conclusions

References

Tables

Figures

◀

▶

◀

▶

Back

Close

Full Screen / Esc

Printer-friendly Version

Interactive Discussion



Abstract

Within the framework of Pliocene Model Intercomparison Project (PlioMIP), the mid-Pliocene (3.264–3.025 Ma) climate simulated by the Flexible Global Ocean-Atmosphere-Land System model grid-point version 2 (FGOALS-g2) are analyzed in 5 this study. Results show that the model reproduces the large-scale features of the global warming over the land and ocean. The simulated mid-Pliocene global annual mean surface air temperature (TAS) and sea surface temperature (SST) are 4.17 and 2.62 °C warmer than the pre-Industrial simulation, respectively. In particular, the feature of larger warming over mid-high latitudes is well captured. In the simulated warm 10 mid-Pliocene climate, the Atlantic Meridional Overturning Circulation (AMOC) and El Niño-Southern Oscillation (ENSO) become weaker.

1 Introduction

The mid-Pliocene (3.264–3.025 Ma BP) is a relatively stable warm period in the geological timescale within the Piacenzian Stage (Dowsett et al., 2010). During this period, 15 the global annual mean surface air temperature (TAS) was estimated approximately 2–3 °C warmer than present climate (Jansen et al., 2007). The ice sheets over Antarctic and Greenland have been reduced (Lunt et al., 2008; Naish et al., 2009; Dolan et al., 2011). The biome reconstruction suggested that the arid deserts decreased at a global extent and the tundra were replaced by forests in the Northern Hemisphere (Salzmann 20 et al., 2008). Coupled model studies show that the meridional and zonal temperature gradients were reduced during mid-Pliocene, which had a significant impact on the Hadley and Walker circulations (Kamae et al., 2011; Contoux et al., 2012). Geological evidences show that the East Asia winter wind was weaker during boreal winter (Jian et al., 2003; Li et al., 2004; Sun et al., 2008; Jiang and Ding, 2010), while the 25 East Asia summer wind was intensified (Ding et al., 2001; Wan et al., 2007), relative to the late Quaternary. The tropical monsoons systems and the East Asian Summer

The mid-Pliocene climate simulated by FGOALS-g2

W. Zheng et al.

[Title Page](#)

[Abstract](#)

[Introduction](#)

[Conclusions](#)

[References](#)

[Tables](#)

[Figures](#)

◀

▶

◀

▶

[Back](#)

[Close](#)

[Full Screen / Esc](#)

[Printer-friendly Version](#)

[Interactive Discussion](#)



The mid-Pliocene
climate simulated by
FGOALS-g2

W. Zheng et al.

Title Page

Abstract

Introduction

Conclusions

References

Tables

Figures

◀

▶

◀

▶

Back Close

Full Screen / Esc

Printer-friendly Version

Interactive Discussion



Monsoon (EASM) may have been enhanced as suggested by the clay mineral records of South China Sea (Wan et al., 2010). Studies of PlioMIP models suggested enhanced East Asian summer wind (EASW) over eastern China and the East Asian winter wind (EAWW) strengthened in southern China but slightly weakened in north monsoon

China (Zhang et al., 2013a), however, inter-model discrepancy is large particularly for the EAWW. The study with atmospheric model showed that the model-data discrepancy in simulating the EAWW at mid-Pliocene may be attributed to the uncertainty in the reconstructed mid-Pliocene sea surface temperature (Yan et al., 2012).

For the ocean climate during the mid-Pliocene, the sea surface temperature (SST) was also warmer, particularly in high latitudes and the North Atlantic (Dowsett et al., 2012), together with a substantially decline in sea-ice cover (Moran et al., 2006; Polyak et al., 2010), and a rise of the sea level from 10 to 45 m above present (Raymo et al., 1996; Miller et al., 2012). The warm North Atlantic surface was often thought to be caused by a much stronger AMOC during the mid-Pliocene (Schmittner et al., 2005), while recent study indicate such warming do not necessitate stronger AMOC (Zhang et al., 2013b). In the tropics, SST gradient across the equatorial Pacific become weaker (Molnar and Cane, 2002; Wara et al., 2005; Ravelo et al., 2006). Permanent El Niño condition was also though to exist in the tropical Pacific during the mid-Pliocene. However, the permanent El Niño condition was not supported by the $\delta^{18}\text{O}$ records from the coral skeletons (Watanabe et al., 2011). Meanwhile, the change of ENSO amplitude relative to preset climate remains unclear. Simulations with the Hadley Centre Coupled Model version 3 (HadCM3) indicated a non-weaker ENSO variability during mid-Pliocene (Haywood et al., 2007; Scroxton et al., 2011). On the contrary, the simulation with the low-resolution version of the Norwegian Earth System Model (NorESM-L) (Zhang et al., 2012) and CCSM4 (Rosenbloom et al., 2012) showed a weaker ENSO during the mid-Pliocene.

Although the mid-Pliocene warm climate has been studied for more than one decade, large debates still exists for key questions of this warm period. In order to further understand the warm mid-Pliocene climate, the Pliocene Model Intercomparison

Title Page

Abstract

Introduction

Conclusions

References

Tables

Figures

◀

▶

◀

▶

Back

Close

Full Screen / Esc

Printer-friendly Version

Interactive Discussion



Project (PlioMIP) was initiated (Haywood et al., 2010, 2011). It was also included in the third phase Palaeoclimate Modeling Intercomparison Project (PMIP3). Within the framework of PlioMIP, atmosphere general circulation models (AGCMs) and coupled general circulation models (CGCMs) are used to simulate the mid-Pliocene climate following the standard experimental protocols. Preliminary results from several models participated in PlioMIP have been published in a special issue of the Journal Geoscientific Model Development (http://www.geosci-model-dev.net/special_issue5.html).

The Flexible Global Ocean-Atmosphere-Land System model grid-point version 2 (FGOALS-g2) also takes part in the PlioMIP. After the hard work for development and validation of the model (Li et al., 2013a), we finish the mid-Pliocene experiment designed in the PlioMIP. In this paper, we describe the experiment, as a contribution to the PlioMIP. The manuscript is organized as follows: Sect. 2 briefly describes the model and the experimental protocols adapted for the mid-Pliocene simulation. Section 3 describes the changes of mid-Pliocene climate compared to the pre-industrial simulation. The major conclusions for the mid-Pliocene simulation of FGOALS-g2 and the model-data discrepancy are summarized in Sect. 4.

2 Model and experimental designs

2.1 Model – FGOALS-g2

The coupled climate model used in this study is the Flexible Global Ocean Atmosphere–Land System model grid-point version 2 (FGOALS-g2) developed at State Key Laboratory of Numerical Modeling for Atmospheric Sciences and Geophysical Fluid Dynamics (LASG), Institute of Atmospheric Physics (IAP), Chinese Academy of Sciences (CAS), which participates in CMIP5 and PMIP3. The model includes four components, the Grid Atmospheric Model of IAP/LASG version 2.0 (GAMIL2.0, Li et al., 2013b), the LASG/IAP Climate system Ocean Model version 2.0 (LICOM2.0, Liu et al., 2012), the improved version based on the CICE (Community Ice CodE) model version

4 named CICE4-LASG (Wang et al., 2010), and the Community Land Model version 3 (CLM3, Oleson et al., 2004). The GAMIL2.0 employs a hybrid horizontal grid, with Gaussian grid of 2.8° between 65.58°S and 65.58°N and weighted equal-area grid poleward of 65.58° and 26 vertical layers up to 0.01 hPa, while LICOM2.0 has a horizontal resolution of $1^\circ \times 1^\circ$ (0.5° meridional resolution in the tropics) and 30 layers in vertical (10 m each layer in the upper 150 m). The resolution of CICE4-LASG and CLM3 is set to the same as the ocean model LICOM2.0 and the atmospheric model GAMIL2.0, respectively. These four components are coupled by the National Center for Atmospheric Research (NCAR) coupler version 6 (CPL6, Craig et al., 2005). Details of FGOALS-g2 are described in Li et al. (2013a). In brief, FGOALS-g2 simulates a better annual cycle of sea surface temperature (SST) along the equatorial Pacific when compared to its previous version. The characteristics of El Niño-Southern Oscillation (ENSO), including the amplitude, period and phase-locking, are well reproduced in the model, as well as the frequency of tropical land precipitation, East Asian Monsoon and the, Madden-Julian oscillation (MJO).

2.2 Experimental designs

The major differences for the experimental protocols between the pre-industrial (PI) and mid-Pliocene simulations are shown in Table 1. The pre-industrial simulation follows the standard experimental protocols of CMIP5, which also serves as the control simulation for the PMIP3. The solar constant is 1365 W m^{-2} and the concentrations of greenhouse gases are set to 280 ppmv for CO₂, 760 ppbv for CH₄ and 270 ppbv for N₂O, respectively.

For the mid-Pliocene experiment, we adapted the protocols of Experiment 2 in PlioMIP, which is designed for the AOGCMs simulations. The detailed boundary conditions was described in Haywood et al. (2011). Due to the challenges in changing the land-sea mask, the alternative dataset of boundary conditions in Experiment 2 is used in our mid-Pliocene simulation. The land-sea mask in the mid-Pliocene is identical to the pre-industrial experiment. The altitude of topography and land surface conditions

6, 2403–2428, 2013

The mid-Pliocene climate simulated by FGOALS-g2

W. Zheng et al.

[Title Page](#)

[Abstract](#)

[Introduction](#)

[Conclusions](#)

[References](#)

[Tables](#)

[Figures](#)

◀

▶

◀

▶

[Back](#)

[Close](#)

[Full Screen / Esc](#)

[Printer-friendly Version](#)

[Interactive Discussion](#)



[Title Page](#)

[Abstract](#)

[Introduction](#)

[Conclusions](#)

[References](#)

[Tables](#)

[Figures](#)

[◀](#)

[▶](#)

[Back](#)

[Close](#)

[Full Screen / Esc](#)

[Printer-friendly Version](#)

[Interactive Discussion](#)



(e.g. vegetation types and ice-sheet) are changed according to the PRISM-3D dataset (Dowsett et al., 2010). The CO₂ concentration is set to 405 ppmv in the mid-Pliocene experiment. Other greenhouse concentrations are prescribed as the same as in the pre-industrial simulation. The ocean model was started by adding the temperature anomalies between PRISM3D dataset and LEVITUS data (Levitus and Boyer, 1994) to the initial field of the ocean temperature. The mid-Pliocene simulation is integrated for 1000 yr. The shortwave radiation at the Top of Model (TOM) and surface air temperature (TAS) have reached equilibrium after a 500-yr spin-up (Fig. 1a, b). The strength of Atlantic Meridional Overtuning Circulation (AMOC) reaches the maximum around the 240 model year and gradually evolves to a stable state (Fig. 1c). The trends of the sea surface temperature (SST) and sea water potential temperature below 1000 m also become very small after several hundreds of simulations (Fig. 1d, e). Therefore, the last 100 yr outputs of the mid-Pliocene simulation are used in this study for the climatology and compared to the PI experiment.

3 Model results

3.1 Changes in atmospheric climatology

3.1.1 Surface Air Temperature (TAS)

The global annual mean TAS for mid-Pliocene is 16.59 °C simulated with the FGOALS-g2, which is 4.17 °C warmer relative to the PI simulation (Table 2). Such warming is larger than the PlioMIP ensemble mean of 2.66 °C as estimated by 8 AOGCMs in Haywood et al. (2013). The pattern of annual mean TAS shows that the warming is relatively small in the tropics, about 1–2 °C warming over the ocean and up to 5 °C over the land (Fig. 2a). The warming is amplified towards mid-high latitudes of both hemispheres, reaching a maximum over Greenland and Antarctica where the ice-sheet are removed. The zonal mean shows that the warming is about 2 °C in the tropics

and increases to about 12 °C and 9 °C in the Northern and Southern Hemisphere, respectively (Fig. 2b), which is within the range of PlioMIP ensemble mean Haywood et al. (2013).

3.1.2 Precipitation

- 5 The global annual mean precipitation increases 0.2 mm d^{-1} ($\sim 7.1\%$) relative to the PI simulation (Table 1). The hydrological cycle in tropics was strengthened at mid-Pliocene as simulated by FGOALS-g2. Enhanced precipitation mainly occurs along the tropical Pacific, Indian Ocean, Indian and West African monsoon regions and mid-high latitudes while reduction of rainfall is observed in the subtropical regions in both hemispheres
- 10 (Fig. 2c). The zonal mean shows that the annual mean precipitation increased about 15 % around 15° N and decreased by 10 % around 30° N and 10° S–30° S, respectively (Fig. 2d). The precipitation were greatly enhanced by more than 15 % beyond 60° S and 60° N in both hemispheres and up to 70 % in the polar regions (Fig. 2d).

3.2 Changes in ocean mean states

3.2.1 SST and sea water potential temperature

15 The global annual mean SST is 2.62 °C warmer at mid-Pliocene relative to the PI simulation (Table 1). The pattern of SST change at mid-Pliocene shows a warming of the entire ocean with the maximum locates over the North Pacific, East Antarctic and parts of North Atlantic (Fig. 3a). The zonal mean of SST shows that the warming of
20 the SST is no more than 5 °C between 40° N and 65° N (Fig. 3b), implying that the warming is more pronounce over the land in the mid-latitudes of Northern Hemisphere (Fig. 1a, b). The warming along the equator is slightly larger in the eastern Pacific than the western Pacific in the mid-Pliocene experiment, indicating that the west-to-east SST gradient remains similar to the PI simulation. Thus the permanent El Niño-like condition as suggested by previous reconstruction studies (Haywood et al., 2013) is

[Title Page](#)[Abstract](#)[Introduction](#)[Conclusions](#)[References](#)[Tables](#)[Figures](#)[◀](#)[▶](#)[◀](#)[▶](#)[Back](#)[Close](#)[Full Screen / Esc](#)[Printer-friendly Version](#)[Interactive Discussion](#)

not significant in mid-Pliocene simulation by FGOALS-g2. The vertical profile of zonal mean sea water potential temperature also shows an entire warming from surface to deep ocean (Fig. 3c). Note that there is an extreme warming in the Arctic basin in the mid-Pliocene simulation, which is related with the bias of inaccurate description of the currents in North Pole that resulted in the trapping of warm salty water in the Arctic basin (Lin et al., 2013). By excluding the extreme warming in the Arctic basin, the warming reaches the maximum in the depth between 1000 and 1500 m, and gradually decreases to a warming of 0.5 °C in the deep ocean (Fig. 3d).

3.2.2 Salinity

- 10 Due to the enhanced hydrological cycle, the global annual mean sea surface salinity (SSS) is decreased by 0.52 psu in the mid-Pliocene experiment (Table 1). The pattern of SSS changes broadly follows the changes in annual precipitation, the SSS decreases over the Indian Ocean, Arctics, the Southern Ocean and the tropical and North Pacific where the increased precipitation locates, while the SSS increases over most parts in the Atlantic Ocean with maximum locate in the tropical and subtropical regions (Fig. 4a). The zonal mean profile of the SSS changes also shows an inverse change relative to the changes in precipitation, decreasing in tropics and high latitudes and increasing in the subtropical regions (Fig. 4b). The vertical profile shows that the salinity mainly increases below 1500 m in the ocean and the regions of North Atlantic Deep Water (Fig. 4c). The extreme salty water mass in the Arctic basin and the fresh water above are related with the model bias as that for the potential temperature. Except the bias, the salinity shows no significant change in the upper ocean and the increasing of salinity is relatively uniform in the ocean below 1500 m (Fig. 4d).

3.2.3 AMOC

- 25 Most model simulations have predicted a weakening of the Atlantic Meridional Overturning Circulation (AMOC) in response to the global warming (Molnar and Cane, 2002;



Wara et al., 2005; Ravelo et al., 2006). However, many studies have pointed to an enhanced AMOC to account for the reconstructions of relatively warm mid-Pliocene SST in the North Atlantic (Schmittner et al., 2005). In the mid-Pliocene simulation of FGOALS-g2, the maximum of AMOC reduces by 1.48 Sv (Table 1). The meridional profile shows that the overturning cell is shallower in the mid-Pliocene experiment (Fig. 5a–c). Thus the northward heat transport is reduced in the North Atlantic (Fig. 5d).

3.3 Changes in the inter-annual variabilities

3.3.1 El Niño-Southern Oscillation (ENSO)

As shown in Fig. 3a, no significant changes in the west-to-east SST gradient can be observed, however, the interannual variation of the SST anomaly in the eastern Pacific is weakened in the mid-Pliocene experiment with the FGOALS-g2. The maximum of variation locates in the Niño3 region, which is similar to the PI simulation (Fig. 6a, b). The Niño 3 index computed from the monthly SST anomalies shows that the amplitude of ENSO reduced by 35 % at mid-Pliocene (Fig. 6c), while the ENSO cycle is slightly lengthened (PI: 3.3 yr; mid-Pliocene: 3.8 yr). The Niño 3.4 index shows a similar reduction of the ENSO amplitude (Fig. 6d). Although the changes in ENSO are not conclusive based on the proxy records and model simulations at present, the results from FGOALS-g2 suggest that the ENSO simulation may be model dependent associated with their different representation of the mean climate and air-sea coupling. In FGOALS-g2, the weakening of ENSO may be associated with the weaker seasonal cycle of the SST in the eastern Pacific (not shown), which needs further analysis.

3.3.2 East Asia Monsoon

The simulation of FGOALS-g2 shows that the northerly winds weaken during boreal winter throughout the East Asia monsoonal regions (Fig. 7b), while the stronger southerly winds related with the East Asia Summer Monsoon prevail over the eastern

[Title Page](#)[Abstract](#)[Introduction](#)[Conclusions](#)[References](#)[Tables](#)[Figures](#)[◀](#)[▶](#)[◀](#)[▶](#)[Back](#)[Close](#)[Full Screen / Esc](#)[Printer-friendly Version](#)[Interactive Discussion](#)



China (Fig. 7d). The stronger southerly winds are mainly associated with the stronger subtropical high located over the western Pacific. The southerly component from the Indian Summer Monsoon is somewhat weakened in the simulation. Both the weaker East Asia Winter Monsoon and stronger East Asia Summer Monsoon are attributed to the enhanced land-sea thermal contrast over East Asia, where the warming over the land is larger than that over the ocean (Fig. 2a).

4 Summary

In this study, we described the mid-Pliocene climate simulated by the FGOALS-g2. Compared to the PI simulation, the model results show that the global annual mean surface air temperature (TAS) was 4.17°C warmer and the annual precipitation was increased by 0.2 mm d^{-1} ($\sim 7.1\%$) (Table 1). The model reproduces the stronger warming in high latitudes, which was mainly due to the removal of ice-sheets. Because of the different thermal inertia of the land and ocean, the warming is relatively larger over the land areas. Thus the thermal contrast between the land and ocean over East Asia was strengthened at mid-Pliocene (Fig. 2a), favoring the strengthening (weakening) of the East Asia Summer (Winter) Monsoon circulation (Fig. 7). Regional changes in precipitation show enhanced hydrological cycle in the tropics, mid-high latitudes and the tropical monsoon regions. Reduction of precipitation mainly occurs in the sub-tropical regions, suggesting the northward shift of the mid-latitude storm tracks (Haywood et al., 2013).

The warming of sea surface temperature (SST) and the deep ocean is also reproduced by FGOALS-g2. Larger warming is simulated in mid-high latitudes in both hemispheres for the SST (Fig. 3a) and between 1000 and 1500 m in the ocean (Fig. 3c). The changes of sea surface salinity (SSS) broadly follow the changes in precipitation in the Pacific and Indian Ocean, while the SSS increases over the most parts in Atlantic (Fig. 4a). The Atlantic Meridional Overturning Circulation (AMOC) slightly weakens at mid-Pliocene (Fig. 5c) that leads to a weaker northward heat transport

Title Page

Abstract

Introduction

Conclusions

References

Tables

Figures

◀

▶

◀

▶

Back

Close

Full Screen / Esc

Printer-friendly Version

Interactive Discussion



(Fig. 5d). The permanent El Niño condition is not obvious in the mid-Pliocene simulation by FGOALS-g2 due to the small changes of zonal SST gradient. However, the model shows a weakening of the interannual variability in eastern tropical Pacific, of which the ENSO amplitude is significantly reduced and the ENSO cycle is slightly lengthened.

5 Data-model biases are found for the SST in the mid-Pliocene simulation by FGOALS-g2 when compared to the PRISM3D reconstruction. Figure 8 shows a broad agreement between data and model result that the differences are limited within the range of $\pm 2^{\circ}\text{C}$, except in the North Atlantic where the model underestimates the changes in SST by 8°C (Fig. 8). Such underestimation was also documented in (Haywood et al.,
10 2013) for other PlioMIP models. In the simulation by FGOALS-g2, the underestimated of SST in the North Atlantic may be associated with the weaker northward heat transport, which needs further studies.

Acknowledgements. This study was jointly supported by the Chinese National Basic Research Program (Grant Nos. 2010CB950502 and 2012CB955202), the National Natural Science Foundation (Grant Nos. 41006008 and 41023002) and the “Strategic Priority Research Program Climate Change: Carbon Budget and Relevant Issues” of the Chinese Academy of Sciences (Grant No. XDA05110301).

References

- Contoux, C., Ramstein, G., and Jost, A.: Modelling the mid-Pliocene Warm Period climate with the IPSL coupled model and its atmospheric component LMDZ5A, Geosci. Model Dev., 5, 903–917, doi:10.5194/gmd-5-903-2012, 2012.
20 Craig, A. P., Jacob, R., Kauffman, B., Bettge, T., Larson, J., Ong, E., Ding, C., and He, Y.: CPL6: the new extensible, high performance parallel coupler for the Community Climate System Model, Int. J. High Perform. C., 19, 309–327, 2005.
25 Ding, Z. L., Yang, S. L., Sun, J. M., and Liu, T. S.: Iron geochemistry of loess and red clay deposits in the Chinese Loess Plateau and implications for long-term Asian monsoon evolution in the last 7.0 Ma, Earth Planet. Sc. Lett., 185, 99–109, doi:10.1016/S0012-821X(00)00366-6, 2001.

The mid-Pliocene climate simulated by FGOALS-g2

W. Zheng et al.

[Title Page](#)

[Abstract](#)

[Introduction](#)

[Conclusions](#)

[References](#)

[Tables](#)

[Figures](#)

◀

▶

◀

▶

[Back](#)

[Close](#)

[Full Screen / Esc](#)

[Printer-friendly Version](#)

[Interactive Discussion](#)



Dolan, A. M., Haywood, A. M., Hill, D. J., Dowsett, H. J., Hunter, S. J., Lunt, D. J., and Pickering, S. J.: Sensitivity of Pliocene ice sheets to orbital forcing, *Palaeogeogr. Palaeocl.*, 309, 98–110, doi:10.1016/j.palaeo.2011.03.030, 2011.

Dowsett, H., Robinson, M., Haywood, A., Salzmann, U., Hill, D., Sohl, L., Chandler, M., Williams, M., Foley, K., and Stoll, D.: The PRISM3D paleoenvironmental reconstruction, *Stratigraphy*, 7, 123–139, 2010.

Dowsett, H. J., Robinson, M. M., Haywood, A. M., Hill, D. J., Dolan, A. M., Stoll, D. K., Chan, W.-L., Abe-Ouchi, A., Chandler, M. A., and Rosenbloom, N. A.: Assessing confidence in Pliocene sea surface temperatures to evaluate predictive models, *Nature Clim. Change*, 2, 365–371, 2012.

Haywood, A. M., Valdes, P. J., and Peck, V. L.: A permanent El Niño-like state during the Pliocene?, *Paleoceanography*, 22, PA1213, doi:10.1029/2006PA001323, 2007.

Haywood, A. M., Dowsett, H. J., Otto-Bliesner, B., Chandler, M. A., Dolan, A. M., Hill, D. J., Lunt, D. J., Robinson, M. M., Rosenbloom, N., Salzmann, U., and Sohl, L. E.: Pliocene Model Intercomparison Project (PlioMIP): experimental design and boundary conditions (Experiment 1), *Geosci. Model Dev.*, 3, 227–242, doi:10.5194/gmd-3-227-2010, 2010.

Haywood, A. M., Dowsett, H. J., Robinson, M. M., Stoll, D. K., Dolan, A. M., Lunt, D. J., Otto-Bliesner, B., and Chandler, M. A.: Pliocene Model Intercomparison Project (PlioMIP): experimental design and boundary conditions (Experiment 2), *Geosci. Model Dev.*, 4, 571–577, doi:10.5194/gmd-4-571-2011, 2011.

Haywood, A. M., Hill, D. J., Dolan, A. M., Otto-Bliesner, B. L., Bragg, F., Chan, W.-L., Chandler, M. A., Contoux, C., Dowsett, H. J., Jost, A., Kamae, Y., Lohmann, G., Lunt, D. J., Abe-Ouchi, A., Pickering, S. J., Ramstein, G., Rosenbloom, N. A., Salzmann, U., Sohl, L., Stepanek, C., Ueda, H., Yan, Q., and Zhang, Z.: Large-scale features of Pliocene climate: results from the Pliocene Model Intercomparison Project, *Clim. Past*, 9, 191–209, doi:10.5194/cp-9-191-2013, 2013.

Jansen, E., Overpeck, J., Briffa, K. R., Duplessy, J.-C., Joos, F., Masson-Delmotte, V., Olago, D., Otto-Bliesner, B., Peltier, W. R., and Rahmstorf, S.: Palaeoclimate, in: *Climate Change 2007: The Physical Science Basis, Contribution of Working Group I to the Fourth Assessment Report of the Intergovernmental Panel on Climate Change* edited by: Solomon, S., Qin, D., Manning, M., Chen, Z., Marquis, M., Averyt, K. B., Tignor, M., and Miller, H. L., Cambridge University Press, Cambridge, UK and New York, NY, USA.

The mid-Pliocene climate simulated by FGOALS-g2

W. Zheng et al.

Title Page

Abstract

Introduction

Conclusion:

References

Tables

Figures

ANSWER

1

10 of 10

1

Back

Clos

1

17

Full Screen / Esc

Related Studies/Materials

Interactive Discussion



- Jian, Z., Zhao, Q., Cheng, X., Wang, J., Wang, P., and Su, X.: Pliocene – Pleistocene stable isotope and paleoceanographic changes in the northern South China Sea, *Palaeogeogr. Palaeocl.*, 193, 425–442, doi:10.1016/S0031-0182(03)00259-1, 2003.

Jiang, H., and Ding, Z.: Eolian grain-size signature of the Sikouzi lacustrine sediments (Chinese Loess Plateau): implications for Neogene evolution of the East Asian winter monsoon, *Geol. Soc. Am. Bull.*, 122, 843–854, doi:10.1130/b26583.1, 2010.

Kamae, Y., Ueda, H., and Kitoh, A.: Hadley and Walker Circulations in the mid-Pliocene warm period simulated by an atmospheric general circulation model, *J. Meteorol. Soc. Jpn.*, 89, 475–493, doi:10.2151/jmsj.2011-505, 2011.

Levitus, S. and Boyer, T. P.: World Ocean Atlas 1994, vol. 4, Temperature, NOAA Atlas NESDIS 4, US Department of Commerce, Washington, DC, 117 pp., 1994.

Li, B., Wang, J., Huang, B., Li, Q., Jian, Z., Zhao, Q., Su, X., and Wang, P.: South China Sea surface water evolution over the last 12 Myr: a south-north comparison from Ocean Drilling Program sites 1143 and 1146, *Paleoceanography*, 19, PA1009, doi:10.1029/2003PA000906, 2004.

Li, L., Lin, P., Yu, Y., Wang, B., Zhou, T., Liu, L., Li, L., Lin, P., Yu, Y., Wang, B., Zhou, T., Liu, L., Liu, J., Bao, Q., Xu, S., Huang, W., Xia, K., Pu, Y., Dong, L., Shen, S., Liu, Y., Hu, N., Liu, M., Sun, W., Shi, X., Zheng, W., Wu, B., Song, M., Liu, H., Zhang, X., Wu, G., Xue, W., Huang, X., Yang, G., Song, Z., and Qiao, F.: The Flexible Global Ocean-Atmosphere-Land System Model: grid-point Version g2: FGOALS-g2, *Adv. Atmos. Sci.*, 30, 543–560, doi:10.1007/s00376-012-2140-6, 2013a.

Li, L., Wang, B., Dong, L., Liu, L., Shen, S., Hu, N., Sun, W., Wang, Y., Huang, W., Shi, X., Pu, Y., and Yang, G.: Evaluation of version two of the grid-point atmospheric model (GAMIL 2.0), *Adv. Atmos. Sci.*, 30, 855–867, doi:10.1007/s00376-013-2157-5, 2013b

Lin, P. F., Yu, Y. Q., and Liu, H. L.: Oceanic climatology in the coupled model FGOALS-g2: improvements and biases, *Adv. Atmos. Sci.*, 30, 819–840, doi:10.1007/s00376-012-2137-1, 2013.

Liu, H. L., Lin, P. F., Yu, Y. Q., and Zhang, X. H.: The baseline evaluation of LASG/IAP Climate system Ocean Model (LICOM) version 2.0, *Acta Meteorol. Sin.*, 26, 318–329, 2012.

Lunt, D. J., Foster, G. L., Haywood, A. M., and Stone, E. J.: Late Pliocene Greenland glaciation controlled by a decline in atmospheric CO₂ levels, *Nature*, 454, 1102–1105, doi:10.1038/nature07223, 2008.

The mid-Pliocene climate simulated by FGOALS-g2

W. Zheng et al.

[Title Page](#)

[Abstract](#)

[Introduction](#)

[Conclusions](#)

[References](#)

[Tables](#)

[Figures](#)

◀

▶

[Back](#)

[Close](#)

[Full Screen / Esc](#)

[Printer-friendly Version](#)

[Interactive Discussion](#)



- Salzmann, U., Haywood, A. M., Lunt, D. J., Valdes, P. J., and Hill, D. J.: A new global biome reconstruction and data-model comparison for the Middle Pliocene, *Global Ecol. Biogeogr.*, 17, 432–447, doi:10.1111/J.1466-8238.2008.00381.X, 2008.
- Schmittner, A., Latif, M., and Schneider, B.: Model projections of the North Atlantic thermohaline circulation for the 21st century assessed by observations, *Geophys. Res. Lett.*, 32, L23710, doi:10.1029/2005GL024368, 2005.
- Scroxton, N., Bonham, S. G., Rickaby, R. E. M., Lawrence, S. H. F., Hermoso, M., and Haywood, A. M.: Persistent El Niño–Southern Oscillation variation during the Pliocene Epoch, *Paleoceanography*, 26, PA2215, doi:10.1029/2010PA002097, 2011.
- Sun, D., Su, R., Bloemendal, J., and Lu, H.: Grain-size and accumulation rate records from Late Cenozoic aeolian sequences in northern China: implications for variations in the East Asian winter monsoon and westerly atmospheric circulation, *Palaeogeogr. Palaeocl.*, 264, 39–53, doi:10.1016/j.palaeo.2008.03.011, 2008.
- Wan, S., Li, A., Clift, P. D., and Stuut, J.-B. W.: Development of the East Asian monsoon: mineralogical and sedimentologic records in the northern South China Sea since 20 Ma, *Palaeogeogr. Palaeocl.*, 254, 561–582, doi:10.1016/j.palaeo.2007.07.009, 2007.
- Wan, S., Tian, J., Steinke, S., Li, A., and Li, T.: Evolution and variability of the East Asian summer monsoon during the Pliocene: evidence from clay mineral records of the South China Sea, *Palaeogeogr. Palaeocl.*, 293, 237–247, doi:10.1016/j.palaeo.2010.05.025, 2010.
- Wang, X. C., Liu, J. P., Yu, Y. Q., and Liu, H. L.: Experiment of coupling sea ice mode CICE4 to LASG/IAP climate system model, *Chinese Journal of Atmospheric Sciences*, 34, 780–792, 2010 (in Chinese).
- Wara, M. W., Ravelo, A. C., and Delaney, M. L.: Permanent El Niño-like conditions during the Pliocene warm period, *Science*, 309, 758–761, doi:10.1126/Science.1112596, 2005.
- Watanabe, T., Suzuki, A., Minobe, S., Kawashima, T., Kameo, K., Minoshima, K., Aguilar, Y. M., Wani, R., Kawahata, H., Sowa, K., Nagai, T., and Kase, T.: Permanent El Niño during the Pliocene warm period not supported by coral evidence, *Nature*, 471, 209–211, 2011.
- Yan, Q., Zhang, Z. S., and Gao, Y. Q.: An East Asian Monsoon in the Mid-Pliocene, *Atmos. Oceanic Sci. Lett.*, 5, 449–454, 2012.
- Zhang, R., Yan, Q., Zhang, Z. S., Jiang, D., Otto-Bliesner, B. L., Haywood, A. M., Hill, D. J., Dolan, A. M., Stepanek, C., Lohmann, G., Contoux, C., Bragg, F., Chan, W.-L., Chandler, M. A., Jost, A., Kamae, Y., Abe-Ouchi, A., Ramstein, G., Rosenbloom, N. A., Sohl, L.,

The mid-Pliocene
climate simulated by
FGOALS-g2

W. Zheng et al.

[Title Page](#)

[Abstract](#)

[Introduction](#)

[Conclusions](#)

[References](#)

[Tables](#)

[Figures](#)

◀

▶

◀

▶

[Back](#)

[Close](#)

[Full Screen / Esc](#)

[Printer-friendly Version](#)

[Interactive Discussion](#)



The mid-Pliocene climate simulated by FGOALS-g2

W. Zheng et al.

[Title Page](#)

[Abstract](#)

[Introduction](#)

[Conclusions](#)

[References](#)

[Tables](#)

[Figures](#)

[|◀](#)

[▶|](#)

[◀](#)

[▶](#)

[Back](#)

[Close](#)

[Full Screen / Esc](#)

[Printer-friendly Version](#)

[Interactive Discussion](#)



**The mid-Pliocene
climate simulated by
FGOALS-g2**

W. Zheng et al.

Table 1. The major differences in the mid-Pliocene experimental designs relative to the pre-Industrial simulation by FGOALS-g2.

	pre-Industrial (PI) simulation	mid-Pliocene simulation
Experiment protocol	CMIP5/PMIP3	Experiment 2 – Alternative
Total length of integration	> 1000 yr	1000 yr
Years used for climatology	Molde year 801–900, 100 yr	Last 100 yr
Ocean initial state	Stationary	Stationary + PRISM3D (Global_dot_v2.0)
Topography	Modern	PRISM3D (topo_v1.1)
Ice sheets and vegetation	Modern	PRISM3D (biome_veg_v1.3)
CO ₂ concentration	280 ppmv	405 ppmv

Discussion Paper | Discussion Paper

[Title Page](#)[Abstract](#)[Introduction](#)[Conclusions](#)[References](#)[Tables](#)[Figures](#)[|◀](#)[▶|](#)[◀](#)[▶](#)[Back](#)[Close](#)[Full Screen / Esc](#)[Printer-friendly Version](#)[Interactive Discussion](#)

The mid-Pliocene climate simulated by FGOALS-g2

W. Zheng et al.

Table 2. Global annual mean values for the atmospheric and oceanic variables in the pre-Industrial and mid-Pliocene simulations. The values for Atlantic Meridional Overturning Circulation (AMOC) are estimated from the maximum stream function.

	Net Radiation at TOM (Wm^{-2})	TAS ($^{\circ}\text{C}$)	Precipitation (mm d^{-1})	SST ($^{\circ}\text{C}$)	SSS (psu)	AMOC (Sv)
0 ka	-0.84	12.42	2.81	17.42	34.96	28.61
3 ma	-0.49	16.59	3.01	20.04	34.44	27.13
3 ma–0 ka	0.35	4.17	0.2	2.62	-0.52	-1.48

[Title Page](#)[Abstract](#)[Introduction](#)[Conclusions](#)[References](#)[Tables](#)[Figures](#)[|◀](#)[▶|](#)[◀](#)[▶](#)[Back](#)[Close](#)[Full Screen / Esc](#)[Printer-friendly Version](#)[Interactive Discussion](#)

The mid-Pliocene climate simulated by FGOALS-g2

W. Zheng et al.

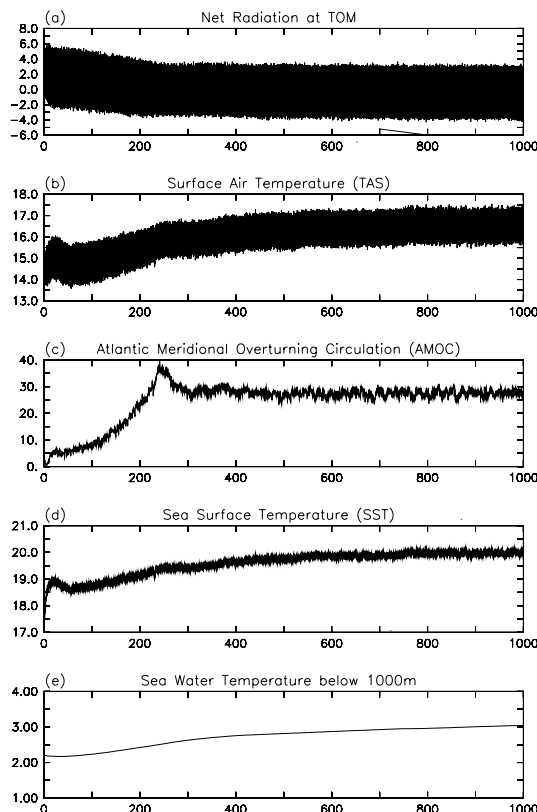


Fig. 1. Time series from the mid-Pliocene simulation of FGOALS-g2 for **(a)** the net shortwave radiation at the Top of Model (TOM, W m^{-2}); **(b)** surface air temperature (TAS, $^{\circ}\text{C}$); **(c)** the maximum of Atlantic Meridional Overturning Circulation (AMOC, Sv); **(d)** sea surface temperature (SST, $^{\circ}\text{C}$) and **(e)** the potential temperature averaged below 1000 m ($^{\circ}\text{C}$).

[Title Page](#)

[Abstract](#)

[Introduction](#)

[Conclusions](#)

[References](#)

[Tables](#)

[Figures](#)

[◀](#)

[▶](#)

[◀](#)

[▶](#)

[Back](#)

[Close](#)

[Full Screen / Esc](#)

[Printer-friendly Version](#)

[Interactive Discussion](#)

The mid-Pliocene climate simulated by FGOALS-g2

W. Zheng et al.

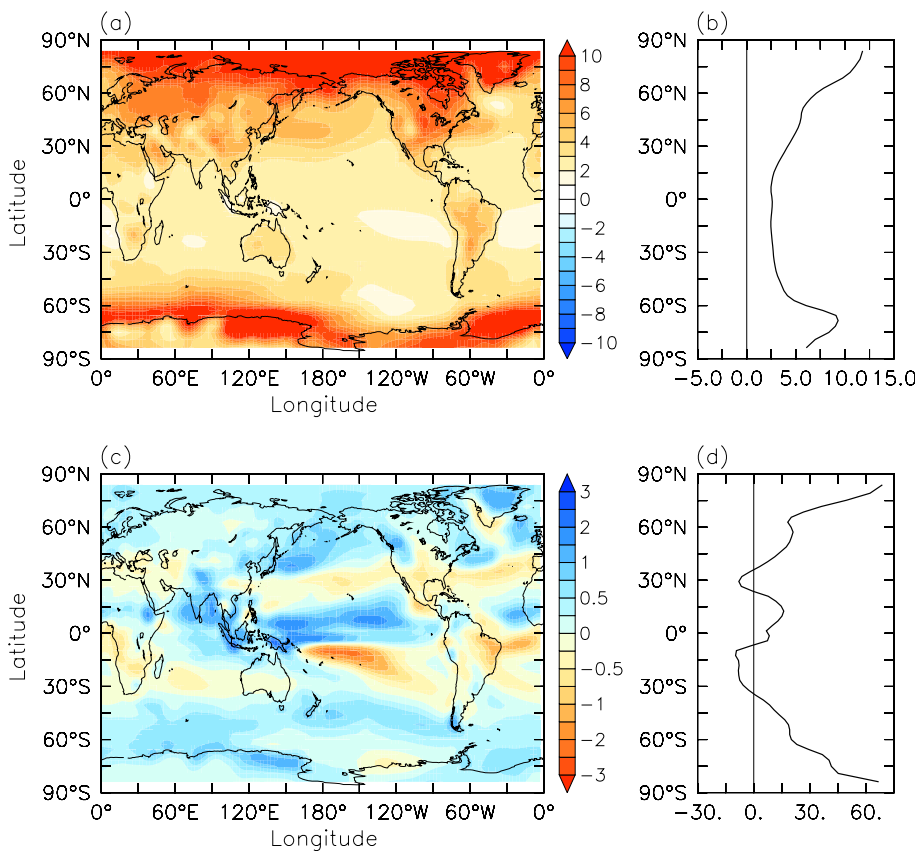


Fig. 2. The differences of annual mean values between the mid-Pliocene and the pre-Industrial simulation (3 ma–0 ka) for **(a)** TAS; **(b)** zonal mean TAS; **(c)** precipitation and **(d)** zonal mean precipitation. The units are $^{\circ}\text{C}$ and mm d^{-1} for the TAS and precipitation, respectively.

The mid-Pliocene climate simulated by FGOALS-g2

W. Zheng et al.

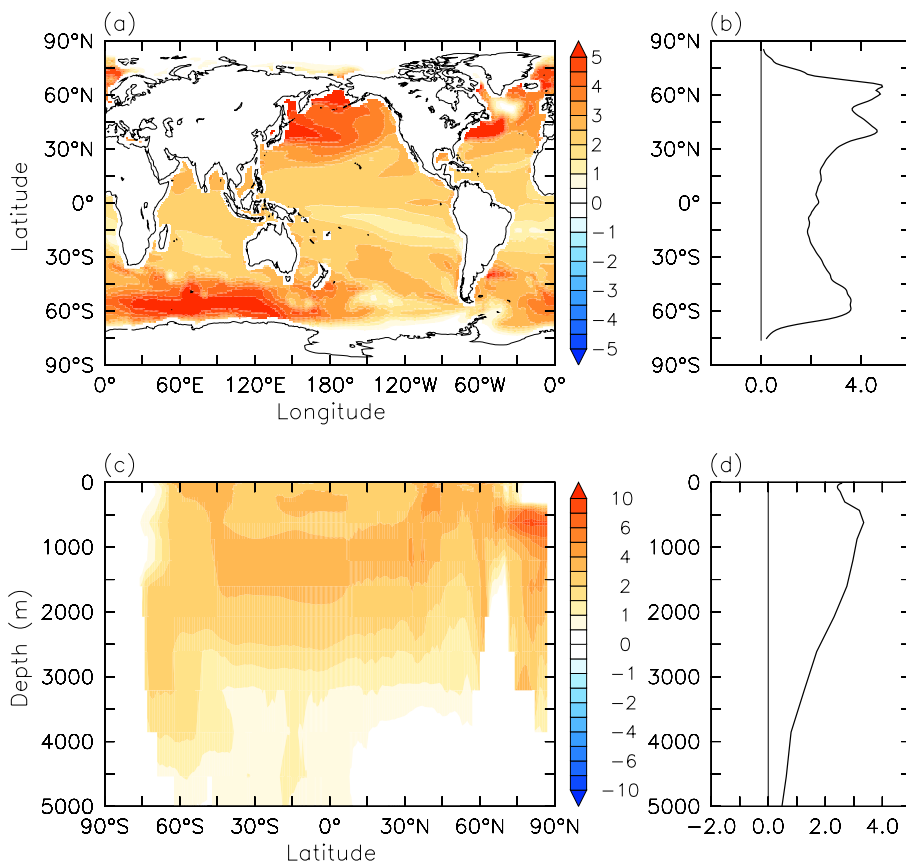


Fig. 3. The differences of annual mean values between the mid-Pliocene and the pre-Industrial simulation (3 ma–0 ka) for **(a)** SST; **(b)** zonal mean SST; **(c)** the sea water potential temperature and **(d)** zonal mean potential temperature. Units: °C.

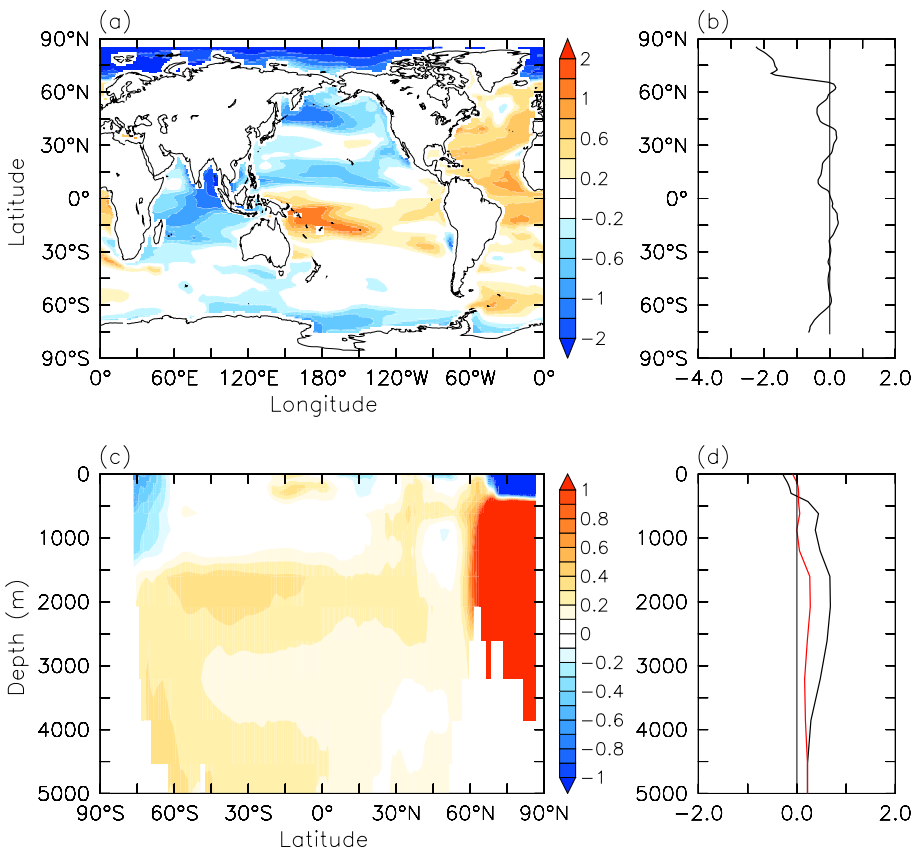


Fig. 4. Same as Fig. 3 but for the changes in salinity. Units: psu. The red line in (d) is estimated by excluding the changes beyond 65° N.

The mid-Pliocene climate simulated by FGOALS-g2

W. Zheng et al.

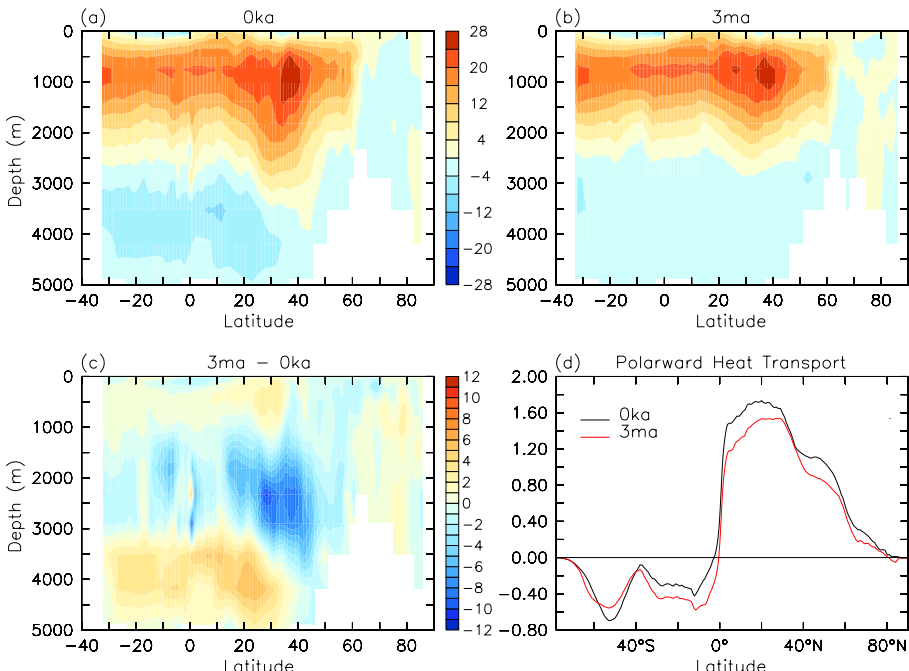


Fig. 5. The stream function for **(a)** pre-Industrial (0 ka) and **(b)** mid-Pliocene (3 ma) simulated by FGOALS-g2; **(c)** the difference between mid-Pliocene and pre-Industrial (3 ma–0 ka); and **(d)** the northward heat transport (PW), black line is for the pre-Industrial and red line for the mid-Pliocene simulation.

Title Page

Abstract

Introduction

Conclusion

References

Tables

Figures



Back

Close

Full Screen / Esc

[Printer-friendly Version](#)

Interactive Discussion



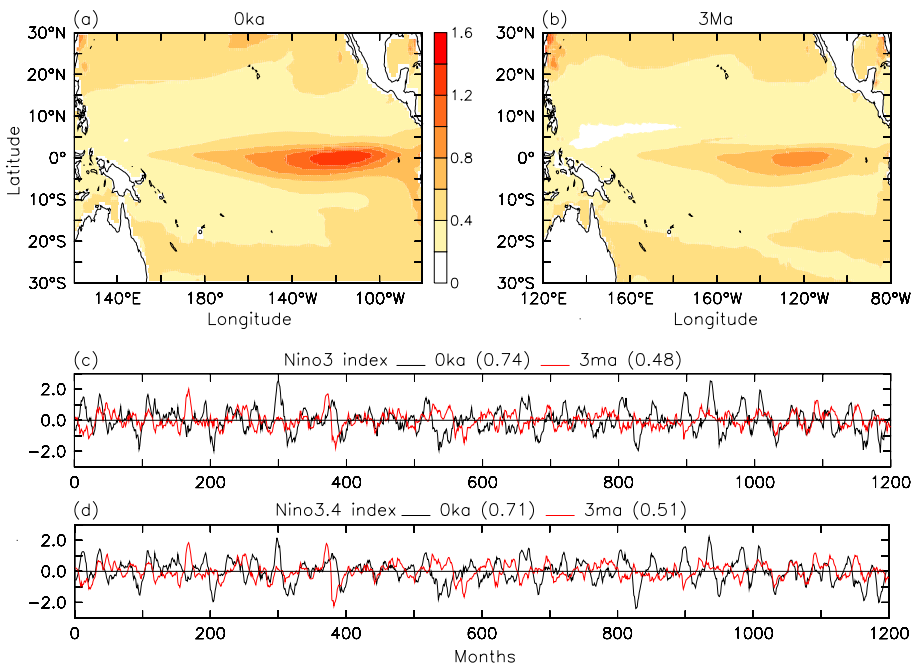


Fig. 6. The standard deviation of the SST anomalies over the tropical Pacific for **(a)** pre-Industrial (0 ka) and **(b)** mid-Pliocene (3 ma); **(c)** the time series of Niño 3 index, black line is for the pre-Industrial and red line for the mid-Pliocene simulation; and **(d)** same as **(c)** but for the Niño 3.4 index. Units: °C.

Title Page

Abstract	Introduction
Conclusions	References
Tables	Figures

1

1

[Back](#)

Full Screen / Esc

[Printer-friendly Version](#)

Interactive Discussion



The mid-Pliocene climate simulated by FGOALS-g2

W. Zheng et al.

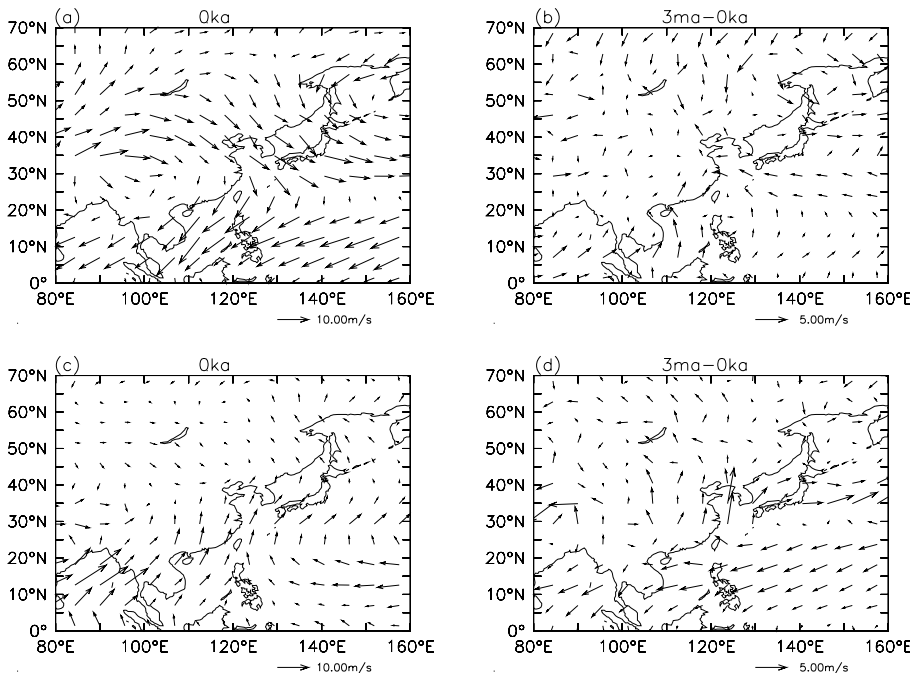


Fig. 7. The atmospheric circulation at the 850 hPa for (a) East Asia Winter winds from pre-Industrial (0 ka); (b) the differences of the winter winds between the mid-Pliocene and pre-Industrial simulation (3 ma–0 ka); (c) and (d) same as (a) and (b) but for the East Asia Summer winds. Units: ms^{-1} .

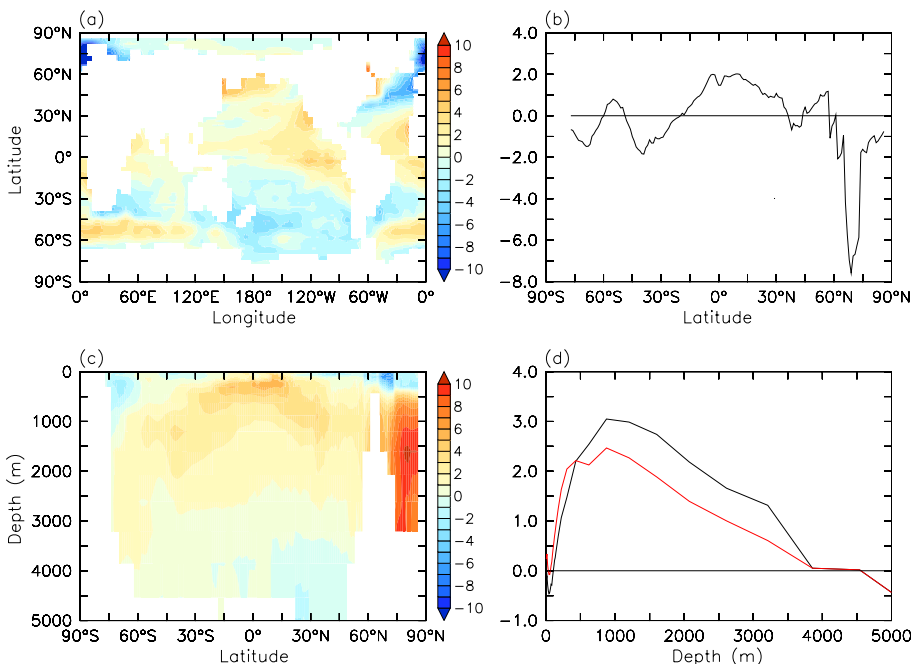


Fig. 8. Same as Fig. 3 but for the differences between the FGOALS-g2 SST and the PRISM3D reconstruction. Units: °C. The red line in (d) is estimated by excluding the changes beyond 65° N.

W. Zheng et al.

[View all posts by admin](#) | [View all posts in category](#)

Title Page

Abstract

Introduction

Conclusion:

References

Conclusions References

References

Tables

Figures

14

▶

1

Back

Close

Full Screen / Esc

[Printer-friendly Version](#)

Interactive Discussion